Applied Physics Letters

RESEARCH ARTICLE | NOVEMBER 27 2024

Detection efficiency characterization for free-space single-photon detectors: Measurement facility and wavelength-dependence investigation

Special Collection: Advances in Quantum Metrology

S. Virzì ; A. Meda ; E. Redolfi ; M. Gramegna ; G. Brida ; M. Genovese ; I. P. Degiovanni

Check for updates

Appl. Phys. Lett. 125, 221108 (2024)
https://doi.org/10.1063/5.0226170

View Online
Export Citation

Articles You May Be Interested In

Interference effects in commercially available free-space silicon single-photon avalanche diodes

Appl. Phys. Lett. (November 2024)

Detection of ultra-weak laser pulses by free-running single-photon detectors: Modeling dead time and dark counts effects

Appl. Phys. Lett. (April 2021)

02 December 2024 15:37:51

AIP Publishing

AIP Publishing
Applied Physics Letters
Special Topics Open for Submissions
Learn More

Applied Physics Letters ARTICLE pubs.aip.org/aip/apl

Detection efficiency characterization for free-space single-photon detectors: Measurement facility and wavelength-dependence investigation

Cite as: Appl. Phys. Lett. **125**, 221108 (2024); doi: 10.1063/5.0226170
Submitted: 29 June 2024 · Accepted: 13 November 2024 ·
Published Online: 27 November 2024

View Online Export Citation CrossMark

S. Virzì,[1,a)] A. Meda,[1] E. Redolfi,[1,2,3] M. Gramegna,[1] G. Brida,[1] M. Genovese,[1,3] and I. P. Degiovanni[1,3]

AFFILIATIONS

[1]Istituto Nazionale di Ricerca Metrologica, str. delle Cacce 91, 10135 Turin, Italy
[2]Physis Department, University of Turin, via P. Giuria 1, 10125 Turin, Italy
[3]Istituto Nazionale di Fisica Nucleare, sez. di Torino, via P. Giuria 1, 10125 Turin, Italy

Note: This paper is part of the APL Special Collection on Advances in Quantum Metrology.
[a)]**Author to whom correspondence should be addressed:** s.virzi@inrim.it

ABSTRACT

In this paper, we present an experimental apparatus for the measurement of the detection efficiency of free-space single-photon detectors based on the substitution method. We extend the analysis to account for the wavelength dependence introduced by the transmissivity of the optical window in front of the detector's active area. Our method involves measuring the detector's response at different wavelengths and comparing it to a calibrated reference detector. This allows us to accurately quantify the efficiency variations due to the optical window's transmissivity. The results provide a comprehensive understanding of the wavelength-dependent efficiency, which is crucial for optimizing the performance of single-photon detectors in various applications, including quantum communication and photonics research. This characterization technique offers a significant advancement in the precision and reliability of single-photon detection efficiency measurements.

© 2024 Author(s). All article content, except where otherwise noted, is licensed under a Creative Commons Attribution (CC BY) license (https://creativecommons.org/licenses/by/4.0/). https://doi.org/10.1063/5.0226170

02 December 2024 15:37:51

The detection of single photons represents a crucial stage in a variety of scientific and technological applications, including quantum communication,[1–3] quantum computing,[4–6] quantum imaging,[7] and quantum sensing[8–11] with photons. Accurate photon detection is essential for ensuring the reliability and precision of these applications. Consequently, the calibration of the detection efficiency of single-photon detectors (SPDs) is of paramount importance.[12–22] Such an efficiency is defined[23] as the probability of a SPD producing a measurable signal in response to one incident photon, depending on the wavelength and detection rate, with specific wavelength and count rate specifications.

However, unlike detectors calibrated using classical radiometric techniques, there is currently no established standard for calibrating the detection efficiency of SPDs based on the measured counts. This lack of standardization presents a significant challenge, as it may hinder the ability to ensure reliable calibration by different labs, leading to incompatible calibration results even if formally traceable to the International System of Units (SI), because of the exploitation of incorrect (as non-standardized) measurement models. For this reason, a pilot study[24] has recently been initiated among various national metrology institutes (NMIs) worldwide to attempt to define a characterization standard for free-space silicon single-photon avalanche diodes (Si-SPADs) detecting photons with a wavelength of 850 nm. This collaborative effort aims to establish a unified and precise methodology for assessing the performance and detection efficiency of these detectors, thereby providing a reliable benchmark for scientific research and technological applications that depend on accurate single-photon detection.

Si-SPADs are SPDs operating in Geiger mode.[25–28] They are widely exploited due to their high detection efficiency in the visible range (up to 80% for wavelengths around 650 nm), their low dark count rate (tens of counts per second), and their short dead time and jitter (typically tens of nanoseconds and hundreds of picoseconds, respectively). They can be exploited for a broad wavelength interval, spanning from approximately 400 nm to 1000 nm. In particular, they find huge application for free-space Quantum Key Distribution (QKD),[29] wherein the employed wavelength is often around 850 nm, because of the transmissivity of the atmosphere just considering the

© Author(s) 2024

range detectable from silicon-based SPDs, that is also the wavelength considered in the pilot study.

The detection efficiency is inherently dependent on the wavelength of the incident photons. In addition, in SPDs operating in free space with an optical window typically made of glass, there can be an additional (nonlinear) dependency on wavelength due to the interference effect that occurs between the two optical surfaces of the window, changing the transmissivity. Glass and quartz windows, while offering high transparency across a broad spectrum, still exhibit such a behavior, acting as an optical cavity, that can affect the overall detection efficiency. These variations must be carefully characterized and accounted for to ensure accurate and reliable photon detection across different wavelengths. Furthermore, there is an ongoing debate about interference effects observed in the spatial responses of these detectors that could significantly impact the detection efficiency (see, e.g., the study carried on at NPL[30]).

In this work, we present the INRiM experimental setup for the measurement of the detection efficiency for free-space SPDs based on the substitution method.[17,19] In particular, we demonstrate such a technique on free-running Si-SPADs at 850 nm in the framework of the aforementioned pilot study. Additionally, we provide a model for the transmissivity of the quartz optical window to account for its impact on the overall detection efficiency.

The substitution method consists of a technique for comparing the signal measured by a SI-traceable detector with respect to the one measured from a SPD after a proper attenuation. This comparison involves light fluxes that differ by several orders of magnitude. For example, a photon flux of about 1000 counts/s with wavelength 850 nm corresponds to an average optical power on the order of 10^{-16} W. Hence, the required attenuation between the high-flux regime and the single-photon level is usually around six or seven orders of magnitude, and it is of the utmost importance to characterize such an attenuation, containing its related uncertainty.

Then, the detection efficiency $\eta(\lambda)$ of a SPD can be estimated comparing the macroscopic optical power $\mathscr{P}$ of a laser source, measured with a SI-traceable calibrated detector, and the rate $\mathscr{R}$ measured by the SPD after attenuating the same signal down to the single-photon level,

$$\eta(\lambda) = \frac{hc}{\lambda}\frac{\mathscr{R}}{\tau\mathscr{P}}, \tag{1}$$

where h is the Planck constant, c is the speed of light in the vacuum, λ is the wavelength of the photons, and τ is the transmissivity due to the introduced attenuation.

In Fig. 1, we show the measurement apparatus. The source is a CW Ti:Sa laser with tunable wavelength. The laser light intensity is controlled by a first variable optical attenuator stage exploiting polarizers and half waveplates. Then, after a mechanical shutter, the laser light is fiber coupled into a single-mode fiber, optimizing the emitting spatial profile, and with two 50:50 beam splitters, it is addressed to a monitor stage for checking both the emission wavelength and optical power stability, and to a second fully pigtailed attenuator stage, which improves repeatability and accuracy of the introduced transmittance with respect to the previous approach implemented at INRiM labs.[19] It consists of two unbalanced beam splitters: the former 999:1, and the latter 9999:1, respectively, allowing introducing a 30 dB and a 40 dB attenuation. The light path is selected thanks to three

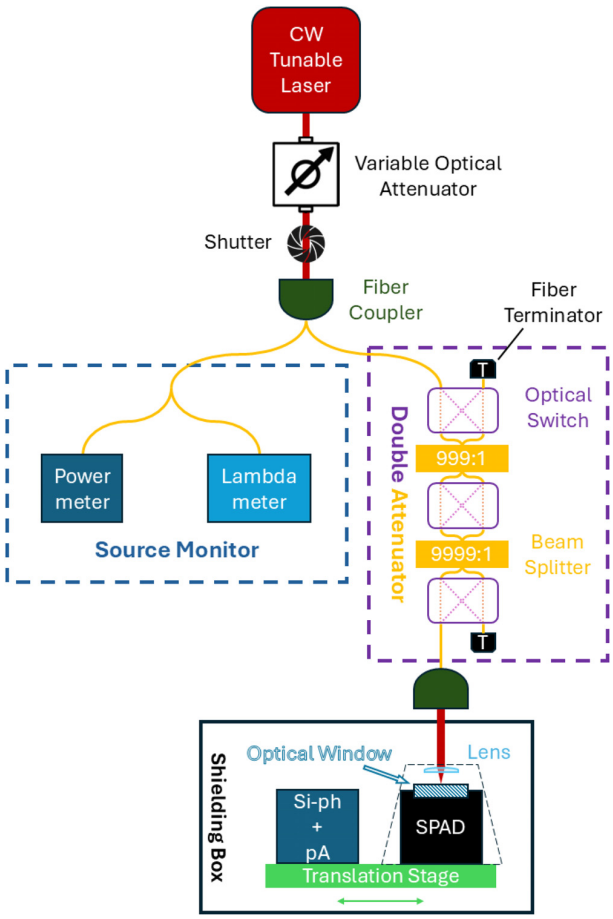

FIG. 1. Experimental setup. The source is a tunable Ti:Sa laser followed by a variable optical attenuator. After a mechanical shutter, photons are fiber-coupled into a single-mode optical fiber through a 20 X microscope objective, and two 50:50 beam splitters direct a part of the photons to a powermeter and a lambdameter for monitoring the source stability. A double attenuator system allows introducing the transmissivity τ, addressing the photons through two unbalanced beam splitters: the former is a 999:1 (30 dB) beam splitter, and the latter is a 9999:1 (40 dB) beam splitter. The selected path is controlled by three optical switches. Then, the output photons are directed through free space into a shielding box, where a motorized stage allows choosing between two detectors: a silicon photodiode (Si-ph) for high-flux measurements and the *quantum* device under test (DUT) consisting of a free-space Si-SPAD in the free-running mode. In front of the latter, photons are focused by a lens ($f = 8$ mm). The whole setup is fully automated and can be controlled through a LabVIEW programmed interface.

pc-controlled optical switches. Selecting the path corresponding to the maximum attenuation (nominal 70 dB), the double-attenuator stage reproduces the transmissivity τ required in Eq. (1). Then, the photons will be out-coupled and collimated in free space with a Gaussian spatial mode to be sent into a shielding box for minimizing environmental photons.

A motorized translation stage allows selecting the measuring detector depending on the introduced attenuation: a windowless

02 December 2024 15:37:51

© Author(s) 2024

SI-traceable silicon photodiode (Si-ph) for the measurements of $\mathscr{P}$, and the Si-SPAD *device under test* (DUT) for the measurement of $\mathscr{R}$, when the attenuation reproduces τ, and the photon flux goes down to the single-photon level.

Since the usual diameter of a free-space Si-SPAD active area is about hundreds of micrometers, a lens focuses the photon spatial distribution on it in a diameter of 40 μm. The DUT position is optimized, exploiting three actuators in the x, y, and z directions. All the devices of the depicted setup are connected to a computer via LabVIEW interface, and the measurement routines are automatized.

The DUT detection efficiency is estimated adapting Eq. (1) to the measurements realized with the experimental apparatus previously described, i.e., comparing the SPAD measurements and the Si-ph output. The SPAD produces a macroscopic pulse for each revealed photon and sends it to the electronics that collects N counts in a time interval t, whereas the Si-ph generates photoelectrons proportionally to the incident optical power with a sensitivity s, and the resulting current is revealed by a picoamperometer with calibration factor C.

The transmissivity τ is pc-controlled, and it has been independently measured (see below). Furthermore, one has to consider also the transmissivity T of the lens in front of the SPAD (see Fig. 1). Finally, taking into account the (intrinsic and environmental) noise level for both the SPAD and the Si-ph measurements (N^{env} and A^{env}), that account for dark counts and background photons as well as for the dark current. For the ith measurement run, Eq. (1) becomes

$$\eta_i(\lambda) = \frac{hc}{\lambda t}\frac{s(N_i - N_i^{\text{env}})}{\tau C(A_i - A_i^{\text{env}})T}. \tag{2}$$

The transmissivity τ is characterized exploiting the Si-ph detector. Our double-attenuator approach enables us to divide the introduced attenuation, which is crucial for maintaining the linear response of the detector. Introducing the entire attenuation at once would compromise this linearity, increasing the related uncertainty and the accuracy and reliability of the experimental data. Furthermore, the first optical switch allows for the evaluation of crosstalk caused by the non-ideal behavior of the optical switches. This approach is far more reproducible than the one previously implemented at INRiM labs[19] and enables a much more rigorous characterization of the transmissivity. Therefore, τ is evaluated as $\tau = \tau_{30\text{dB}}\tau_{40\text{dB}}$, where

$$\tau_{x_{dB}} = \frac{A_{x\text{dB}} - A^{\text{env}}}{A_{0\text{dB}} - A^{\text{env}}}, \tag{3}$$

where the subscript x indicates the selected attenuation by the optical switches (see Fig. 1), and the crosstalk contribution is accounted inside A^{env}.

In our experiment, we characterize the behavior of a free-running Si-SPAD with a circular active area of 200 μm in diameter with light at the wavelength of $\lambda = (850.711 \pm 0.006)$ nm. Several factors can reduce the detection efficiency of the SPAD, especially with varying photon wavelengths. These include non-perpendicular incidence of photons on the detector's sensitive area, misalignment, and distorted spatial distribution of photons, among others. For this reason, the experimental setup must typically be carefully aligned and optimized to provide the best possible detection efficiency for the detector under the given conditions.

Since the active area of a commercial free-space detector is generally not uniform, it is necessary to scan it to find a quite flat region. Figure 2 shows that the surface of the active area is relatively uniform except for two dips located on the left side of the scan.

Once the DUT position is fixed far from the two dips, we start the procedure for obtaining the DUT detection efficiency. First of all, we characterize τ [Eq. (3)] averaging over a sequence of 100 measurements. Then, we repeat ten times the τ characterization over different days, i.e., evaluating the repeatability behavior of our double-attenuator system, obtaining $\tau = (2.1601 \pm 0.0070) \times 10^{-7}$, highlighting a reasonable repeatability of our system day by day.

We underline that our double-attenuator approach allows good repeatability since it does not require to disconnect the optical fibers. To monitor the source stability, we exploit the powermeter measurements at the source monitor stage (see Fig. 1). This allows us to correct the measured N_i and A_i in Eqs. (2) and (3) with respect to the source fluctuations according to

$$\begin{aligned} N_i &\to N_i' = N_i \rho_i^{\text{DUT}}, \\ A_i &\to A_i' = \varepsilon A_i \rho_i^{\text{Si-ph}}, \end{aligned} \tag{4}$$

where $\rho_i^{\text{DUT}} = \langle P_i^{\text{DUT}} \rangle / P_i^{\text{DUT}}$ represents the correction with respect to the monitor powermeter measurement P occurring during the ith run of the DUT measurement N_i, meaning $\langle X_i \rangle$ the average value of the variable X; the same argument holds for $\rho_i^{\text{Si-ph}}$. Furthermore, since an imbalance may happen between the average source optical power emission during the DUT and the Si-ph measurements, we have introduced the parameter $\varepsilon = \langle P_i^{\text{DUT}} \rangle / \langle P_i^{\text{Si-ph}} \rangle$.

To remove the arbitrary dependence on the count rate, we estimate the zero-flux efficiency η_0, i.e., the detection efficiency extrapolated to the zero-flux level, whose value is not affected by the presence of the SPD dead time. The behavior of the detection efficiency can be described as[28,31,32,34]

$$\eta_\lambda(\langle N_i' \rangle) = \eta_0 - D\frac{\langle N_i' - N_{\text{env}} \rangle}{t}, \tag{5}$$

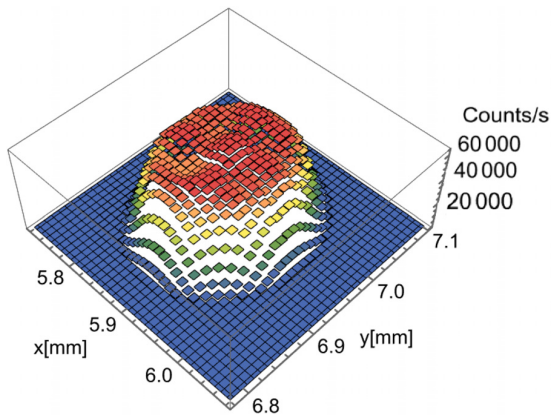

FIG. 2. (300 × 300) μm^2 scan of the Si-SPAD's active area obtained by setting a step size of 0.01 mm in both the directions transversal to the photons propagation. The distance with respect to the focal lens was previously optimized and fixed obtaining a focused beam with waist around 40 μm.

02 December 2024 15:37:51

© Author(s) 2024

where D is the dead time, and N_i' is defined in Eq. (4). The detection efficiency $\eta_\lambda(\langle N_i' \rangle)$ varies with the photon count rate due to the detector's dead time D, making this effect noticeable only at high count rates (see Ref. 19 for more details). Hence, estimating $\eta_\lambda(\langle N_i' \rangle)$ for different photon fluxes, η_0 comes out from a linear regression.

We measured the DUT detection efficiency [according to Eq. (2)] at different photon fluxes acting on the variable attenuator depicted in Fig. 1, obtaining various count-rate regimes from 5000 to 2×10^6 counts/s. The upper photon flux was set one order of magnitude below the detector's maximum count rate to prevent excessive strain on the detector. After collecting ten data points, we perform the linear regression as described in Eq. (5) to estimate η_0. The results are shown in Fig. 3.

As shown in Fig. 3, the experimental results align well with the fitted behavior. From the presented measurement run, we obtained $\eta_0 = 0.5526 \pm 0.0029$ (considering the standard measurement uncertainty). Uncertainties are propagated from Eq. (2), considering both statistical and non-statistical contributions. An example of uncertainty budget for a fixed count rate is reported in Table I. Our approach demonstrates the possibility to measure the DUT detection efficiency in a SI-traceable manner, maintaining a contained uncertainty. To assess the robustness of our technique, we repeat the entire estimation process ten times. The results are illustrated in Fig. 4. Once more, the resulting estimations of η_0 exhibit strong agreement. The average value obtained for the detection efficiency at zero-photon flux is $\langle \eta_0 \rangle = 0.5510 \pm 0.0030$. This consistency across multiple estimations underlines the robustness and reliability of our measurement technique.

Finally, we investigate the detection efficiency as a function of photon wavelength. To accomplish this, we replicate the estimation of $\langle \eta_i(\lambda) \rangle$ [Eq. (2)] maintaining a constant $N' \simeq 10^5$, while varying the emission wavelength of our source. The value of N' is arbitrarily chosen, and it represents a reasonable trade-off between reduced distortion effect due to SPD dead time and efficient data collection. The experimental data present a peculiar sinusoidal behavior (see Fig. 5) that we interpret as an etaloning effect of the two surfaces of the optical window of the SPAD packaging, whereas the exploited reference detector is windowless. Indeed, for a window with thickness L and refractive index n, the transmissivity depends on the wavelength λ through the parameter Γ, that is,[33]

$$\Gamma(\lambda, n, L) = \frac{\gamma\left(1 - \exp\left[-2i\frac{2\pi}{\lambda}nL\right]\right)}{1 - \gamma^2 \exp\left[-2i\frac{2\pi}{\lambda}nL\right]}, \tag{6}$$

where $\gamma = (n - n_a)/(n + n_a)$ and n_a represents the air refractive index. Then, the overall detection efficiency in Eq. (2) can be generalized as

$$\eta_i(\lambda, n, L) = \eta_i(\lambda)(1 - |\Gamma(\lambda, n, L)|^2). \tag{7}$$

The results of this analysis are presented in Fig. 5.

Our proposed model aligns closely with the experimental data. In this nonlinear regression, following the SPAD manufacturer's specifications, we set the refractive index to that of quartz ($n = 1.4525$) and the thickness to the nominal value of $L = 100\,\mu$m. Moreover, these

TABLE I. Uncertainty budget related to the detection efficiency [see Eq. (2)] $\langle \eta_i(N', \lambda) \rangle$, with $N' = 20\,655 \pm 27$, showed in Fig. 3.

Coefficient	Value	Uncertainty	% Contribution
N'	20 655	27	5.47
N^{env}	28	1	0.012
A'	$1.928\,07 \times 10^{-8}$ A	4.9×10^{-12} A	0.06
A^{env}	4.88×10^{-14} A	1.3×10^{-15} A	1.5×10^{-8}
τ	$2.160\,1 \times 10^{-7}$	7.0×10^{-10}	33.83
ε	1.014 8	1.4×10^{-3}	5.70
s	0.476 6 W/A	1.9×10^{-3} W/A	51.55
C	1.000 023	1.0×10^{-5}	3.2×10^{-4}
T	0.985 000	3.0×10^{-5}	3.0×10^{-3}
λ	$8.507\,11 \times 10^{-7}$ m	6×10^{-12} m	1.6×10^{-4}
t	1.000 0 s	1.0×10^{-3} s	3.22
$\langle \eta(N', \lambda) \rangle$	0.551 4	0.0031	

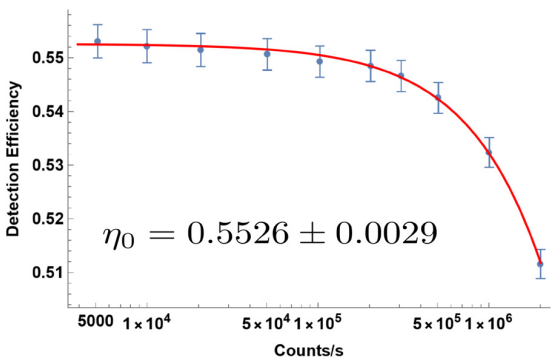

FIG. 3. Detection efficiency estimation for different count rates $\mathscr{R} = \langle N_i' - N_i^{\text{env}} \rangle / t$. The blue dots represent the calculated detection efficiencies with their related uncertainties, as determined by Eq. (2), while the red line is the result of the linear regression according to Eq. (5). η_0 is obtained as the intercept of the fit with the y-axis. All the shown uncertainties consider the standard measurement uncertainty.

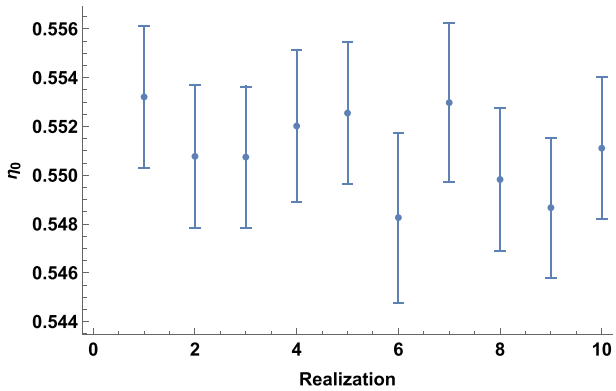

FIG. 4. Si-SPAD detection efficiencies at zero-photon flux (η_0) obtained from ten independent estimations with related standard measurement uncertainties.

02 December 2024 15:37:51

© Author(s) 2024

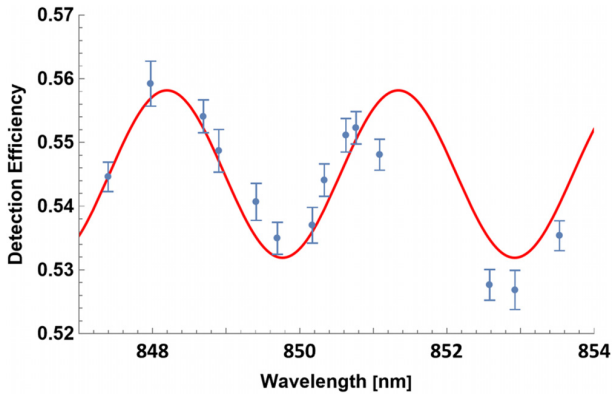

FIG. 5. Characterization of detection efficiency as a function of wavelength. The number of detected photons for each acquisition lasting $t = 1$ s was fixed at approximately $N' \simeq 10^5$ counts. The blue dots represent the experimental results with their associated standard measurement uncertainties, while the red line corresponds to the fitted model described by Eq. (7).

findings highlight the non-negligible impact of transmittance effects caused by the optical window. Within a range of approximately 3 nm, the detection efficiency varies by up to 5%. Consequently, it is imperative from a metrological perspective to consider such effects when characterizing free-space SPADs, rather than only focusing on a single wavelength.

In this work, we presented the INRiM experimental setup for the measurement of the detection efficiency of free-space SPDs, exploiting the substitution method. Specifically, the fully computer-controlled pigtailed attenuation stage optimizes the detection efficiency measurement time thanks to excellent reproducibility, minimizing the uncertainty contribution associated with the attenuation measurement. Then, we extended our analysis to the variation of the detection efficiency as a function of wavelength, taking into account the transmissivity of the optical window positioned in front of the detector's sensitive area. This comprehensive characterization is crucial for optimizing the performance of Si-SPADs in various applications, including quantum communication and photonics research. By understanding the wavelength dependence and the influence of the optical window, we can better estimate the efficiency of these detectors, leading to improved accuracy and reliability in single-photon detection. This study provides a valuable foundation for future metrological characterizations of Si-SPAD technology in both scientific and industrial contexts.

This work was financially supported in the context of the following projects: Qu-Test project, which has received funding from the European Union's Horizon Europe Research and Innovation Program under Grant Agreement No. 101113901; the QUID (QUantum Italy Deployment) and EQUO (European QUantum ecOsystems) projects, which are funded by the European Commission in the Digital Europe Programme under Grant Agreement Nos. 101091408 and 101091561; MIUR-PNRR Italian project, founded by the European Union - NextGenerationEU; the Project No. G6026 SPS NATO; and the EMPIR projects 19NRM06 METISQ and 23NRM04 NoQTeS. The Project Nos. 19NRM06 and 23NRM04 NoQTeS have received funding from the European Partnership on Metrology, co-financed from the European Union's Horizon Europe Research and Innovation Programme and by the participating states.

AUTHOR DECLARATIONS

Conflict of Interest

The authors have no conflicts to disclose.

Author Contributions

S. Virzì: Conceptualization (supporting); Data curation (lead); Formal analysis (equal); Methodology (equal); Software (lead); Writing – original draft (lead); Writing – review & editing (equal). **A. Meda:** Conceptualization (equal); Data curation (equal); Formal analysis (equal); Investigation (equal); Methodology (equal); Supervision (equal); Validation (lead); Writing – original draft (equal); Writing – review & editing (equal). **E. Redolfi:** Data curation (equal); Investigation (supporting); Methodology (supporting); Software (equal). **M. Gramegna:** Conceptualization (equal); Formal analysis (equal); Funding acquisition (equal); Project administration (equal); Writing – original draft (supporting); Writing – review & editing (equal). **G. Brida:** Conceptualization (lead); Formal analysis (equal); Funding acquisition (equal); Investigation (equal); Methodology (equal); Project administration (equal); Resources (equal); Supervision (equal); Validation (equal); Writing – review & editing (equal). **M. Genovese:** Conceptualization (equal); Formal analysis (equal); Funding acquisition (equal); Investigation (equal); Project administration (equal); Resources (equal); Supervision (equal); Writing – original draft (supporting); Writing – review & editing (equal). **I. P. Degiovanni:** Conceptualization (equal); Data curation (equal); Formal analysis (lead); Funding acquisition (lead); Investigation (lead); Methodology (equal); Project administration (equal); Supervision (lead); Validation (equal); Writing – original draft (equal); Writing – review & editing (lead).

DATA AVAILABILITY

The data that support the findings of this study are available from the corresponding author upon reasonable request.

REFERENCES

[1] V. Zapatero, T. van Leent, R. Arnon-Friedman, W.-Z. Liu, Q. Zhang, H. Weinfurter, and M. Curty, "Advances in device-independent quantum key distribution," npj Quantum Inf. **9**, 10 (2023).
[2] E. Diamanti, H.-K. Lo, B. Qi, and Z. Yuan, "Practical challenges in quantum key distribution," npj Quantum Inf. **2**, 16025 (2016).
[3] S. Pirandola, U. L. Andersen, L. Banchi, M. Berta, D. Bunandar, R. Colbeck, D. Englund, T. Gehring, C. Lupo, C. Ottaviani, J. L. Pereira, M. Razavi, J. S. Shaari, M. Tomamichel, V. C. Usenko, G. Vallone, P. Villoresi, and P. Wallden, "Advances in quantum cryptography," Adv. Opt. Photonics **12**, 1012–1236 (2020).
[4] T. D. Ladd, F. Jelezko, R. Laflamme, Y. Nakamura, C. Monroe, and J. L. O'Brien, "Quantum computers," Nature **464**, 45–53 (2010).
[5] S. S. Gill, A. Kumar, H. Singh, M. Singh, K. Kaur, M. Usman, and R. Buyya, "Quantum computing: A taxonomy, systematic review and future directions," Software Pract. Exp. **52**, 66–114 (2022).
[6] P. Krantz, M. Kjaergaard, F. Yan, T. P. Orlando, S. Gustavsson, and W. D. Oliver, "A quantum engineer's guide to superconducting qubits," Appl. Phys. Rev. **6**, 021318 (2019).

02 December 2024 15:37:51

© Author(s) 2024

[7]M. Genovese, "Real applications of quantum imaging," J. Opt. **18**, 073002 (2016).
[8]C. L. Degen, F. Reinhard, and P. Cappellaro, "Quantum sensing," Rev. Mod. Phys. **89**, 035002 (2017).
[9]N. Aslam, H. Zhou, E. K. Urbach, M. J. Turner, R. L. Walsworth, M. D. Lukin, and H. Park, "Quantum sensors for biomedical applications," Nat. Rev. Phys. **5**, 157–169 (2023).
[10]S. Bakhshandeh, "Quantum sensing goes bio," Nat. Rev. Mater. **7**, 254–254 (2022).
[11]G. Petrini, E. Moreva, E. Bernardi, P. Traina, G. Tomagra, V. Carabelli, I. P. Degiovanni, and M. Genovese, "Is a quantum biosensing revolution approaching? perspectives in NV-assisted current and thermal biosensing in living cells," Adv. Quantum Technol. **3**, 2000066 (2020).
[12]A. L. Migdall, R. Datla, A. Sergienko, J. Orszak, and Y. Shih, "Absolute detector quantum-efficiency measurements using correlated photons," Metrologia **32**, 479 (1995).
[13]A. Migdall, S. Castelletto, I. P. Degiovanni, and M. L. Rastello, "Intercomparison of a correlated-photon-based method to measure detector quantum efficiency," Appl. Opt. **41**, 2914–2922 (2002).
[14]A. Ghazi-Bellouati, A. Razet, J. Bastie, M. Himbert, I. Degiovanni, S. Castelletto, and M. L. Rastello, "Radiometric reference for weak radiations: Comparison of methods," Metrologia **42**, 271 (2005).
[15]S. V. Polyakov and A. L. Migdall, "Quantum radiometry," J. Mod. Opt. **56**, 1045–1052 (2009).
[16]C. J. Chunnilall, I. P. Degiovanni, S. Kück, I. Müller, and A. G. Sinclair, "Metrology of single-photon sources and detectors: A review," Opt. Eng. **53**, 081910 (2014).
[17]M. López, H. Hofer, and S. Kück, "Detection efficiency calibration of single-photon silicon avalanche photodiodes traceable using double attenuator technique," J. Mod. Opt. **62**, 1732–1738 (2015).
[18]I.-H. Bae, S. Park, K.-S. Hong, H. S. Park, H. J. Lee, H. S. Moon, J. S. Borbely, and D.-H. Lee, "Detection efficiency measurement of single photon avalanche photodiodes by using a focused monochromatic beam tunable from 250 nm to 1000 nm," Metrologia **56**, 035003 (2019).
[19]M. López, A. Meda, G. Porrovecchio, R. Starkwood, M. Genovese, G. Brida, M. Šmid, C. Chunnilall, I. Degiovanni, and S. Kück, "A study to develop a robust method for measuring the detection efficiency of free-running InGaAs/InP single-photon detectors," EPJ Quantum Technol. **7**, 14 (2020).
[20]T. Gerrits, A. Migdall, J. C. Bienfang, J. Lehman, S. W. Nam, J. Splett, I. Vayshenker, and J. Wang, "Calibration of free-space and fiber-coupled single-photon detectors," Metrologia **57**, 015002 (2020).
[21]H. Georgieva, M. López, H. Hofer, N. Kanold, A. Kaganskiy, S. Rodt, S. Reitzenstein, and S. Kück, "Absolute calibration of a single-photon avalanche detector using a bright triggered single-photon source based on an InGaAs quantum dot," Opt. Express **29**, 23500–23507 (2021).
[22]J. Jin, T. Gerrits, and A. Gamouras, "Calibration and comparison of detection efficiency for free-space single-photon avalanche diodes at 850 nm," Appl. Opt. **61**, 5244–5249 (2022).
[23]J. C. Bienfang, J. Bienfang, T. Gerrits, P. Kuo, A. Migdall, S. Polyakov, and O. T. Slattery, Single-*Photon Sources* and *Detectors Dictionary* (US Department of Commerce, National Institute of Standards and Technology, 2023).
[24]See https://www.bipm.org/en/committees/cc/ccpr/wg/ccpr-wg-sp-tg11 for "Pilot study website."
[25]D. Bronzi, F. Villa, S. Tisa, A. Tosi, and F. Zappa, "SPAD figures of merit for photon-counting, photon-timing, and imaging applications: A review," IEEE Sens. J. **16**, 3–12 (2016).
[26]F. Villa, F. Severini, F. Madonini, and F. Zappa, "SPADs and SiPMs arrays for long-range high-speed light detection and ranging (LiDAR)," Sensors **21**, 3839 (2021).
[27]C. Bruschini, H. Homulle, I. M. Antolovic, S. Burri, and E. Charbon, "Single-photon avalanche diode imagers in biophotonics: Review and outlook," Light Sci. Appl. **8**, 87 (2019).
[28]A. Migdall, S. V. Polyakov, J. Fan, and J. C. Bienfang, *Single-Photon Generation and Detection: Physics and Applications* (Academic Press, 2013).
[29]M. A. Nielsen and I. L. Chuang, *Quantum Computation and Quantum Information* (Cambridge university Press Cambridge, 2001), Vol. 2.
[30]L. Arabskyj, B. Dejen, T. S. Santana, M. Lucamarini, C. J. Chunnilall, and P. R. Dolan, "Interference effects in commercially-available free-space silicon single-photon avalanche diodes," private communication (2024).
[31]S. Castelletto, I. P. Degiovanni, and M. L. Rastello, "Theoretical aspects of photon number measurement," Metrologia **37**, 613 (2000).
[32]G. Brida, M. Genovese, and C. Novero, "An application of two-photon entangled states to quantum metrology," J. Mod. Opt. **47**, 2099–2104 (2000).
[33]H. A. Macleod and H. A. Macleod, *Thin-Film Optical Filters* (CRC Press, 2010).
[34]G. Brida, M. Genovese, and M. Gramegna, "Twin-photon techniques for photo-detector calibration," Laser Phys. Lett. **3**, 115 (2006).

02 December 2024 15:37:51

© Author(s) 2024